J. KSIAM Vol.18, No.2, 181–192, 2014 http://dx.doi.org/10.12941/jksiam.2014.18.181

A LOCALIZED GLOBAL DEFORMATION MODEL TO TRACK MYOCARDIAL MOTION USING ECHOCARDIOGRAPHY

CHI YOUNG AHN

DIVISION OF COMPUTATIONAL MATHEMATICS, NATIONAL INSTITUTE FOR MATHEMATICAL SCIENCES, DAEJEON 305-811, SOUTH KOREA

E-mail address: chiyoung@nims.re.kr

ABSTRACT. In this paper, we propose a robust real-time myocardial border tracking algorithm for echocardiography. Commonly, after an initial contour of LV border is traced at one or two frame from the entire cardiac cycle, LV contour tracking is performed over the remaining frames. Among a variety of tracking techniques, optical flow method is the most widely used for motion estimation of moving objects. However, when echocardiography data is heavily corrupted in some local regions, the errors bring the tracking point out of the endocardial border, resulting in distorted LV contours. This shape distortion often occurs in practice since the data acquisition is affected by ultrasound artifacts, dropout or shadowing phenomena of cardiac walls. The proposed method deals with this shape distortion problem and reflects the motion realistic LV shape by applying global deformation modeled as affine transform partitively to the contour. We partition the tracking points on the contour into a few groups and determine each affine transform governing the motion of the partitioned contour points. To compute the coefficients of each affine transform, we use the least squares method with equality constraints that are given by the relationship between the coefficients and a few contour points showing good tracking results. Many real experiments show that the proposed method supports better performance than existing methods.

1. INTRODUCTION

The automated analysis of left ventricle (LV) using echocardiography is steadily demanding for medical assessment including motion analysis and strain analysis. Most of analysis methods are based on LV measurements in two-dimensional (2D) slices, because they are available in clinical practice [1, 2]. The LV measurements are commonly performed by manually drawing endocardial border in some 2D slices (such as end-systole (ES) or end-diastole (ED) frames) selected from the entire cardiac cycle and automatically tracking the traced LV contour over the remaining frames [3, 4]. This tracking process is accomplished by observing the speckle

Received by the editors April 25 2014; Accepted May 21 2014; Published online June 2 2014.

2000 *Mathematics Subject Classification.* 68U10, 92C50.

Key words and phrases. Echocardiography, Left ventricle, Speckle tracking, Affine transform, Least squares with equality constraints.

This work was supported by the National Research Foundation of Korea (NRF) and the National Institute for Mathematical Sciences(NIMS) grants funded by the Korea government(No. NRF-2012R1A1A2038700 and NIMS-A21402).

pattern, which is inherent appearance associated with soft tissues in ultrasound imaging and reflects the local echogeneity of the underlying scatterers. However, it is a difficult task to automatically track the motion of endocardial border in echocardiography data due to artifacts, shadowing phenomena, low-contrast and so on. User intervention is hence required for stable and successful tracking of endocardial border.

In the last two decades, there have been a variety of studies to trace LV wall motion using the tracking methods such as deformable models [5–8], active shape models [9–11], optical flow methods [2, 12–15], and so on. Nevertheless, they still have some limitations according to practical application to endocardial border motion in ultrasound images. The tracking methods based on deformable models or active shape models are somewhat inadequate for strain analysis related to local motion and deformation of heart, because they are not speckle tracking-based methods providing motion information of local region on the myocardium but shape-based tracking methods. They thus provide only the information of moving LV border and enable user to measure the volume inside LV. On the other hand, optical flows provide the local motion information of myocardium and are capable of measuring the LV volume as well as the myocardial wall motion analysis or strain analysis to detect LV abnormalities. But, some problems arise in cases of ultrasound images with unclear speckle pattern or weak signals. In practical environment, the contour points tracked by optical flows often present some inaccurate results due to above-mentioned ultrasound artifacts, dropouts or shadowing phenomena of cardiac wall [16]. For example, in the presence of edge dropout or indistinguishable speckle pattern in a local neighborhood of a tracking point, optical flows bring the tracking point out of the endocardial border, resulting in distorted LV contours or irregular distances between the tracked points throughout the entire cardiac cycle. These distorted results adversely affect LV volume measurement or strain analysis.

Among several attempts to overcome those difficulties, Sühling *et al.* [13] proposed a tracking method based on the weighted window Lucas-Kanade(LK) method [17], which estimated the displacements by minimizing the weighted least square criterion in the neighborhood of each tracking point. In their method, a linear model of multiple frames centering around the given time t for the velocity along the time direction was used and more robust results were showed than that of the weighted LK method using the single frame at t. Compared with the approaches based on the LK method, Duan *et al.* [15] used the region-based tracking method (also known as the block matching or pattern matching method) with the cross-correlation coefficients as a similarity measure that is less sensitive to noise, fast motion and potential occlusions and discontinuities. However, these tracking methods still have drawback in dealing with the problem of the contour shape distortion in the presence of locally weak signal corrupted by rib shadowing and other factors.

In order to alleviate the LV shape distortion, we recently proposed a new optical flow method equipped with a global motion constraint [18]. It was designed to prevent each tracking point from getting out of the endocardial border by incorporating the LK optical flow method and a global motion constraint being approximately an affine transformation of the initial tracking points into a variational framework. Nevertheless, it still needs to be improved to deal with flexible and practical cardiac wall motion.

This paper proposes a new tracking algorithm that satisfies the requirements to alleviate the LV shape distortion and reflect realistic motion of endocardial contour. We consider both of global and local deformations of non-rigid heart motion by applying global deformation modeled as affine transform to the contour partitively. It is carried out by partitioning the tracking points on the contour into a few small groups and determining each affine transform governing the motion of the partitioned contour points. To compute the coefficients of each affine transform, we solve a least squares problem with equality constraints that are given by the relationship between the coefficients and a few contour points showing good tracking results. Numerical experiments show that the proposed method achieves better tracking performance compared to our previous algorithm [18] that outperforms the block matching tracking methods and the LK optical flows.

2. METHODS

2.1. **Proposed method.** Typically, heart motion is regarded as the non-rigid motion by rotation, contraction/expansion and shear [19, 20]. This non-rigid motion consists of global deformation modeled by an affine transformation and local deformation described by a free-form deformation. In order to reflect the global and local deformations of the endocardial motion simultaneously, we divide the whole tracking points into a few groups. Especially, each group is selected to include the tracking points located on a shadowing endocardial region disconnected by edge dropout and to be controlled by individual affine transform. Through the separated affine transforms, we compensate their poorly tracking results and perform the non-rigid motion of LV contour efficiently.

Let the endocardial border traced at initially selected frame (for example, end-systole or end-diastole frame) denoted by a parametric contour $\mathcal{C}^* = \{\mathbf{r}^*(s) = (x^*(s), y^*(s)) \mid 0 \le s \le 1\}$ that can be identified as its n tracking points $\mathbf{r}_1^* = \mathbf{r}^*(s_1), \cdots, \mathbf{r}_n^* = \mathbf{r}^*(s_n)$. Here, $0 = s_1 < s_2 < \cdots < s_n = 1$. Let $\mathcal{C}(t) = \{\mathbf{r}(s,t) = (x(s,t), y(s,t)) \mid 0 \le s \le 1\}$ be the contour deformed from $\mathcal{C}(0) = \mathcal{C}^*$ at time t. The motion of the contour $\mathcal{C}(t)$ will be determined by an appropriately chosen velocity $\mathbf{U}(t)$ indicating a time change of tracking points $(\mathbf{r}_1(t), \cdots, \mathbf{r}_n(t))$:

$$\mathbf{U}(t) := \begin{bmatrix} \mathbf{u}_1(t) \\ \vdots \\ \mathbf{u}_n(t) \end{bmatrix} = \frac{d}{dt} \begin{bmatrix} \mathbf{r}_1(t) \\ \vdots \\ \mathbf{r}_n(t) \end{bmatrix} \qquad \text{with} \qquad \begin{bmatrix} \mathbf{r}_1(0) \\ \vdots \\ \mathbf{r}_n(0) \end{bmatrix} = \begin{bmatrix} \mathbf{r}_1^* \\ \vdots \\ \mathbf{r}_n^* \end{bmatrix}$$

Here, we identify the contour $\mathcal{C}(t)$ with tracking points $\{\mathbf{r}_1(t), \cdots, \mathbf{r}_n(t)\}$ and regard each point $\mathbf{r}_i$ as column vector.

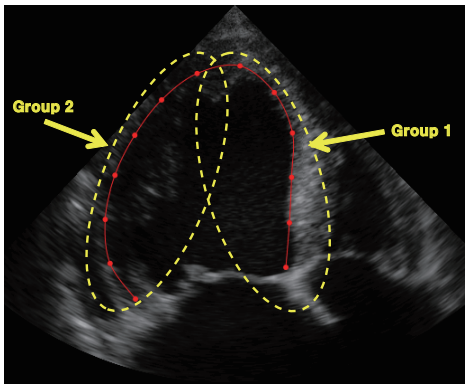

FIGURE 1. An example partitioning 13 control points into two groups. Some tracking points in the second group are located on the contour with weak edges.

For the tracking method mentioned above, we let the set of tracking points $\{\mathbf{r}_1(t), \cdots, \mathbf{r}_n(t)\}$ be partitioned into M groups as follows:

$$\begin{aligned} G_1 =& \{\mathbf{r}_{k_0}(t), \mathbf{r}_{k_0+1}(t), \cdots, \mathbf{r}_{k_1-1}(t), \mathbf{r}_{k_1}(t)\}, \\ G_2 =& \{\mathbf{r}_{k_1}(t), \mathbf{r}_{k_1+1}(t), \cdots, \mathbf{r}_{k_2-1}(t), \mathbf{r}_{k_2}(t)\}, \\ & \cdots \\ G_M =& \{\mathbf{r}_{k_{M-1}}(t), \mathbf{r}_{k_{M-1}+1}(t), \cdots, \mathbf{r}_{k_M-1}(t), \mathbf{r}_{k_M}(t)\}, \end{aligned}$$

where $1 = k_0 < k_1 < \cdots < k_{M-1} < k_M = n$ and $\mathbf{r}_{k_0}(t), \mathbf{r}_{k_1}(t), \cdots, \mathbf{r}_{k_M}(t)$ mean the tracking points for obvious speckle patterns by strong signals so that they become one of both ends of each group of tracking points. That is, we assume that the displacements $\mathbf{u}_{k_0}(t), \mathbf{u}_{k_1}(t), \cdots, \mathbf{u}_{k_M}(t)$ are reliable results computed by a commonly used speckle tracking method. Since the apex and two annulus regions of endocardial borders are usually represented as good edges by strong signals, we set the number of groups to 2. Fig. 1 shows an example of 13 control points partitioned into two groups ($n = 13$ and $M = 2$). Using these partitions of tracking points, the proposed tracking method is performed as follows.

We apply the optical flows tracking method [17] to compute the displacements $\mathbf{u}_1(t)$,$\cdots$, $\mathbf{u}_n(t)$. By solving the least squares method with equality constraints that are given by the relationship between the initial points $\mathbf{r}^*_{k_0}, \mathbf{r}^*_{k_1}, \cdots, \mathbf{r}^*_{k_M}$ and the displacements $\mathbf{u}_{k_0}(t)$,$\mathbf{u}_{k_1}(t)$,$\cdots$, $\mathbf{u}_{k_M}(t)$, we determine the coefficients $a_{1,j}, \cdots, a_{6,j}$ of affine transform corresponding to each group G_j $(j = 1, \cdots, M)$ and compute the displacements of the remaining tracking points except for both ends in each group G_j again using the determined affine transform and all the initial points belonging to G_j. The proposed method is capable of compensating the poorly tracking points near endocardium with unclear speckle patterns or edge dropout by utilizing the tracking points reflecting well-tracking results by optical flows tracking method as well as applying local deformation effects.

To sum up, the proposed tracking method is performed as follows.

1. Select the first frame from the whole image frames for a heartbeat cycle.
2. If current image is the last one, go to step 3. or perform the following process:
   (1) Partition the tracking points $\{\mathbf{r}_1(t), \cdots, \mathbf{r}_n(t)\}$ into M groups. (Set $M = 2$ in our application.)
   (2) Compute the displacements $\mathbf{u}_1(t), \cdots, \mathbf{u}_n(t)$ using the optical flows tracking method [17] as a commonly used speckle tracking method.
   (3) Solve the least squares problem with equality constraints to determine the affine transform corresponding to each group of tracking points.
   (4) Compute the displacements of the remaining tracking points except for both ends in each group G_j again using the determined affine transform and all the initial points belonging to G_j.
   (5) Move to next image frame and go to step 2.
3. Terminate the process.

Additionally, we describe how to compute the affine transform corresponding to each group of tracking points in the next subsection.

2.2. **Regional affine transform.** Let the matrix $\begin{bmatrix} \mathbf{r}^*_{k_{j-1}}{}^T & 1 \\ \vdots & \vdots \\ \mathbf{r}^*_{k_j}{}^T & 1 \end{bmatrix}$ be denoted by $\Phi_j(\mathcal{C}^*)$. If the ith point $\mathbf{r}_i(t)$ on LV contour belongs to the jth group G_j of the tracking points, the relationship between the initial points and displacements associated to G_j are represented as the following equations:

$$\Phi_j(\mathcal{C}^*) \begin{bmatrix} a_{1,j}(\mathbf{U}_j(t)) & a_{3,j}(\mathbf{U}_j(t)) \\ a_{2,j}(\mathbf{U}_j(t)) & a_{4,j}(\mathbf{U}_j(t)) \\ a_{5,j}(\mathbf{U}_j(t)) & a_{6,j}(\mathbf{U}_j(t)) \end{bmatrix} = \begin{bmatrix} (\mathbf{r}_{k_{j-1}}(t) + \mathbf{u}_{k_{j-1}}(t))^T \\ \vdots \\ (\mathbf{r}_{k_j}(t) + \mathbf{u}_{k_j}(t))^T \end{bmatrix} \text{ with } \mathbf{U}_j(t) := \begin{bmatrix} \mathbf{u}_{k_{j-1}}(t) \\ \vdots \\ \mathbf{u}_{k_j}(t) \end{bmatrix}. \tag{2.1}$$

We solve the linear equation (2.1) using the least squares method with equality constraints that are given by the equations associated with the both ends $\mathbf{r}_{k_{j-1}}$ and $\mathbf{r}_{k_j}$ of the jth group G_j:

$$\begin{bmatrix} \mathbf{r}^*_{k_{j-1}}{}^T & 1 \\ \mathbf{r}^*_{k_j}{}^T & 1 \end{bmatrix} \begin{bmatrix} a_{1,j}(\mathbf{U}) & a_{3,j}(\mathbf{U}) \\ a_{2,j}(\mathbf{U}) & a_{4,j}(\mathbf{U}) \\ a_{5,j}(\mathbf{U}) & a_{6,j}(\mathbf{U}) \end{bmatrix} = \begin{bmatrix} (\mathbf{r}_{k_{j-1}}(t) + \mathbf{u}_{k_{j-1}})^T \\ (\mathbf{r}_{k_j}(t) + \mathbf{u}_{k_j})^T \end{bmatrix}. \tag{2.2}$$

The description of the least squares method with equality constraints is given in Appendix.

We denote the matrix $\begin{bmatrix} \mathbf{r}^*_{k_{j-1}}{}^T & 1 \\ \mathbf{r}^*_{k_j}{}^T & 1 \end{bmatrix}$ by B and compute the QR-factorization of its transpose matrix B^T as follows:

$$B^T = Q \begin{bmatrix} R \\ 0\,0 \end{bmatrix},$$

where Q is a 3×3 matrix of the form $Q = \begin{bmatrix} \mathbf{q}_1 & \mathbf{q}_2 & \mathbf{q}_3 \end{bmatrix}$ and R is a 2×2 matrix defined by $\begin{bmatrix} r_{11} & r_{12} \\ 0 & r_{22} \end{bmatrix}$.

Let A_1 and A_2 be the matrices defined by

$$A_1 := \Phi_j(\mathcal{C}^*) \begin{bmatrix} \mathbf{q}_1 & \mathbf{q}_2 \end{bmatrix} \text{ and } A_2 := \Phi_j(\mathcal{C}^*)\mathbf{q}_3, \text{ respectively.}$$

Then the coefficients $a_{1,j}(\mathbf{U}), \cdots, a_{6,j}(\mathbf{U})$ are determined by the equations

$$\begin{bmatrix} a_{1,j}(\mathbf{U}) & a_{3,j}(\mathbf{U}) \\ a_{2,j}(\mathbf{U}) & a_{4,j}(\mathbf{U}) \\ a_{5,j}(\mathbf{U}) & a_{6,j}(\mathbf{U}) \end{bmatrix} = Q \begin{bmatrix} R^{-T} \begin{pmatrix} \mathbf{r}_{k_{j-1}} \\ \mathbf{r}_{k_j} \end{pmatrix} \\ (A_2^T A_2)^{-1} A_2^T \left(\begin{pmatrix} \mathbf{r}_{k_{j-1}} \\ \vdots \\ \mathbf{r}_{k_j} \end{pmatrix} - A_1 R^{-T} \begin{pmatrix} \mathbf{r}_{k_{j-1}} \\ \mathbf{r}_{k_j} \end{pmatrix} \right) \end{bmatrix}, \tag{2.3}$$

where R^{-T} means the inverse matrix of R^T.

3. Experimental results

We tested the performance of the proposed algorithm in clinical setting using many real data. The proposed algorithm was compared with our previous algorithm [18] that outperforms the block matching tracking methods and the LK optical flows. For experiments, we used the 10 cases of 420×512 size 2D echocardiography data acquired using a Samsung Medison V10 ultrasound system (Seoul, Korea) and a phased array transducer P2-4BA (2-4 MHz). Each method was performed to track both of the endocardial and epicardial borders simultaneously using 26 tracking points. After that, LV contour was made by connecting the points using the natural cubic spline. We used the standard finite difference method to compute $\mathbf{u} \cdot \nabla I + \frac{\partial}{\partial t} I$ of optical flows method. All the experiments were conducted using MATLAB 8.0 and computer (Intel Core i7-3770 CPU at 3.40 GHz and 16GB RAM) and the computational time was about 9 milliseconds at each frame.

In order to describe that the proposed method shows better performance than the previous method, we selected a representative case among the 10 cases of 2D echocardiography data. The LV tracking results on the representative case were depicted in Fig. 2. The LV border shown in the chosen case includes outer wall part of weak edges. Two contours were initially traced along the inside and outside of LV myocardial wall for endocardial and epicardial borders. Each contour was identified with 26 points. The first row shows manually traced LV contours by a clinical expert for images at ED, ES and next ED frames within the entire cycle. The next two rows exhibit the tracking results obtained by two tracking methods of our previous method and the proposed method. Overall, both of two tracking methods have tracked well dealing with the edge dropouts by weak signals. However, the performance difference was shown in the third column of Fig. 2. The contour obtained by performing the previous method did not reflect the endocardial border sufficiently, while the proposed method has tracked well

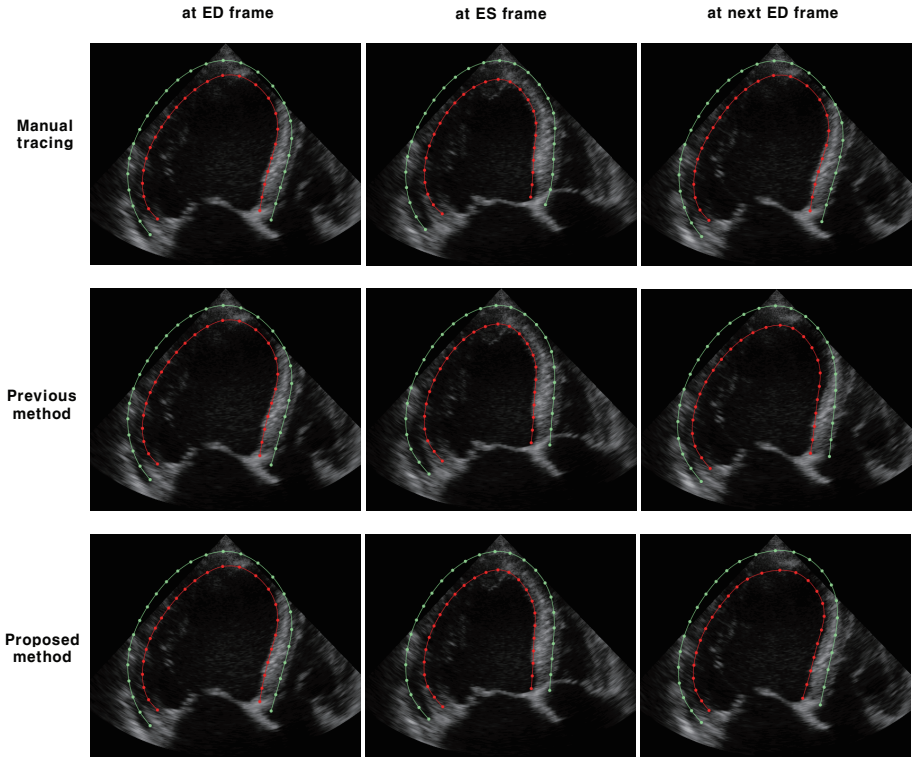

FIGURE 2. Tracking results of the previous and proposed methods compared to manual tracing in sequential image frames. The first column represents initialized contours that are traced at ED phase to perform the tracking algorithms. (The inner red and outer green lines mean endocardial and epicardial borders, respectively.) The second and third columns show the contours obtained by each method at the ES and the next ED frames, respectively. Each row exhibits the tracking results by manual tracing, the previous method and the proposed method from top to bottom, respectively.

the endocardial border very approximately compared to the manual tracing contour. The proposed method kept regular distribution of tracking points and successfully have tracked local speckle patterns.

3.1. **Assessment of LV border tracing.** For quantitative evaluation of the performance of the proposed tracking algorithm, we used the Hausdorff distance ε_H [27, 28] to compare the automated LV contours produced by algorithms with manually traced contours by a clinical expert. Here, the Hausdorff distance between the contour $\mathcal{C}_1$ and $\mathcal{C}_2$ is given by

$$\varepsilon_H(\mathcal{C}_1, \mathcal{C}_2) = \max\left\{ \sup_{\mathbf{r}_1 \in C_1} \left(\min_{\mathbf{r}_2 \in C_2} \|\mathbf{r}_1 - \mathbf{r}_2\| \right) , \sup_{\mathbf{r}_2 \in C_2} \left(\min_{\mathbf{r}_1 \in C_1} \|\mathbf{r}_1 - \mathbf{r}_2\| \right) \right\}.$$

Fig. 3 shows the Hausdorff distances ε_H between contours drawn manually and contours generated automatically for the entire cycle from an ED frame to the next ED frame. For the case used in Fig. 2, the Hausdorff distances ε_H were computed for the whole heartbeat cycle. Blue dotted and red solid lines present the Hausdorff distances ε_H computed for the tracking results of the previous and proposed tracking methods, respectively. We observed that the proposed method provides the smaller errors compared to the previous tracking.

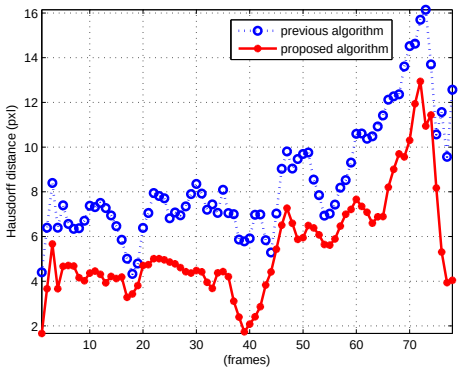

FIGURE 3. Comparison of tracking performance using the Hausdorff distance ε_H. For the case used in Fig. 2, the Hausdorff distance ε_H between the LV contours produced by two tracking methods and reference contours by manually tracing in the whole of images are computed.

3.2. **Assessment of tracking errors for individual point.** For more detailed performance evaluation of the proposed algorithm, we used an additional assessment method regarding on repeatability of local point along the forward and backward entire cardiac cycle. It was proposed in our previous work [18]. Let t_R be a time interval of one heartbeat cycle from ED frame to the next ED frame. Using one cycle image $I(\mathbf{r}, t)$, $0 \le t \le t_R$, we generate a forward-backward image defined by

$$\tilde{I}(\mathbf{r}, t) = \begin{cases} I(\mathbf{r}, t) & \text{if } 0 \le t \le t_R \\ I(\mathbf{r}, 2t_R - t) & \text{if } t_R \le t \le 2\, t_R \end{cases}.$$

Let $\{\mathbf{r}_1^{**}, \cdots, \mathbf{r}_n^{**}\}$ be the set of tracking points returned at time $t = 2t_R$ by performing an automated tracking algorithm on the forward-backward image $\tilde{I}(\mathbf{r}, t)$.

Using the forward-backward image $\tilde{I}(\mathbf{r}, t)$, $0 \le t \le 2t_R$ and the returning tracking position $\mathbf{r}_j^{**}$ at time $t = 2t_R$, we computed local tracking errors defined by the distance between the initial position $\mathbf{r}_j^{*}$ and the corresponding returning position $\mathbf{r}_j^{**}$:

$$\text{Returning Tracking Error (RTE)} \;=\; \sqrt{\frac{1}{n}\sum_{i=1}^{n} |\mathbf{r}_i^{*} \;-\; \mathbf{r}_i^{**}|^2}. \tag{3.1}$$

For the representative case shown in Fig. 2, we obtained the RTE values of 1.3123 and 0.8134 pixels corresponding to the tracking results by previous and proposed methods, respectively. That is, both of overall and regional assessments of tracking results by using ε_H and RTE support that the proposed method outperforms the previous method.

Method	Mean of errors	standard deviation of errors
Previous method	2.2432	0.7037
Proposed method	1.0364	0.5648

TABLE 1. Comparison of tracking performance using the RTE. For the total experimental data set of 10 cases, the RTE values of the contour points produced by the two tracking algorithms are measured. (in pixels)

We computed the RTE values of the tracking points produced by the two tracking algorithms for the experimental data set of 10 cases. In Table 1, the mean and standard deviation of the RTEs obtained by the previous method and the proposed method were described. Table 1 presented that the proposed method provides improved performance compared with the conventional tracking methods.

4. DISCUSSION AND CONCLUSION

In this paper, we proposed a new tracking algorithm that satisfies simultaneously the requirements to alleviate the LV shape distortion and reflect realistic motion of endocardial contour. In order to improve the performance of our previous method related to detailed LV motion, we considered both of global and local deformations of non-rigid heart motion by applying global deformation modeled as affine transform to the contour partitively. It is carried out by partitioning the tracking points on the contour into a few small groups and determining each affine transform governing the motion of the partitioned contour points. To compute the coefficients of each affine transform, we modeled a least squares problem with equality constraints that are given by the relationship between the coefficients and a few contour points showing good tracking results. By doing this, the proposed method keeps regular distribution of tracking points and tracks local speckle patterns successfully by applying local deformation effects as well as compensating the poorly tracking points near endocardium with unclear speckle patterns or edge dropout by utilizing the tracking points reflecting well-tracking results by optical flows tracking method.

We have experimentally demonstrated that the proposed method is capable of performing robust real-time LV border tracking even in the presence of indistinguishable portions of the LV walls in echocardiography data. Especially, the numerical experiments showed that the proposed method achieves better tracking performance compared to our previous algorithm [18] that outperforms commonly used tracking methods including the block matching tracking methods and the LK optical flows.

We used the performance evaluation method for LV tracking that is based on the forward-backward tracking error estimation RTE as shown in section 3.2. The conventional evaluation

of global tracking performance using the delineated LV contours have some limitations in estimating errors of individual tracking points; in the case when tracking points erroneously move along LV border, the LV contour connecting the tracking points can not reveal those individual tracking errors. The forward-backward point tracking error estimation RTE provides a better local tracking performance assessment in the whole cycle.

APPENDIX

Least Squares with Equality Constraints. For $A \in \mathbb{R}^{m\times n}$, $B \in \mathbb{R}^{p\times n}$, $\mathbf{b} \in \mathbb{R}^m$, $\mathbf{d} \in \mathbb{R}^p$, $rank(B) = p$, a constrained least square problem is expressed as a least squares problem with a solution $\mathbf{x}^*$:

$$\mathbf{x}^* = \min_{\mathbf{x}} \|A\mathbf{x} - \mathbf{b}\|_2 \tag{4.1}$$

with equality constraints:

$$B\mathbf{x} = \mathbf{d}. \tag{4.2}$$

To solve this constrained least square problem, we compute the QR-factorization of B^T:

$$B^T = Q \begin{bmatrix} R \\ \mathbf{0} \end{bmatrix} \tag{4.3}$$

with

$$Q \in \mathbb{R}^{n\times n}, R \in \mathbb{R}^{p\times p} \text{ and } \mathbf{0} \in \mathbb{R}^{(n-p)\times p}.$$

And then we consider the following identities:

$$AQ = [A_1 A_2], Q^T\mathbf{x} = \begin{bmatrix} \mathbf{y} \\ \mathbf{z} \end{bmatrix} \text{ with } A_1 \in \mathbb{R}^{n\times p} \text{ and } A_2 \in \mathbb{R}^{n\times(n-p)}. \tag{4.4}$$

Using these identities, we compute $B\mathbf{x}$ and $A\mathbf{x}$:

$$B\mathbf{x} = \left(Q \begin{bmatrix} R \\ \mathbf{0} \end{bmatrix}\right)^T \mathbf{x} = \begin{bmatrix} R^T\mathbf{0} \end{bmatrix} Q^T\mathbf{x} = \begin{bmatrix} R^T\mathbf{0} \end{bmatrix} \begin{bmatrix} \mathbf{y} \\ \mathbf{z} \end{bmatrix} = R^T\mathbf{y} \tag{4.5}$$

and

$$A\mathbf{x} = (AQ)\left(Q^T\mathbf{x}\right) = [A_1 A_2] \begin{bmatrix} \mathbf{y} \\ \mathbf{z} \end{bmatrix} = A_1\mathbf{y} + A_2\mathbf{z}. \tag{4.6}$$

The problem given in the form of (4.1) hence becomes

$$\min_{\mathbf{y},\mathbf{z}} \|A_1\mathbf{y} + A_2\mathbf{z} - \mathbf{b}\|_2 = \min_{\mathbf{y},\mathbf{z}} \|A_2\mathbf{z} - (\mathbf{b} - A_1\mathbf{y})\|_2 \tag{4.7}$$

subject to

$$R^T\mathbf{y} = \mathbf{d}. \tag{4.8}$$

Since $\mathbf{y}$ is determined directly by (4.8), we can find the solution $\mathbf{z}$ of the least square problem (4.7) and finally obtain

$$\mathbf{x} = Q \begin{bmatrix} \mathbf{y} \\ \mathbf{z} \end{bmatrix}.$$

ACKNOWLEDGMENTS

We would like to thank Samsung Medison R&D Center for supporting many ultrasound data and valuable suggestions.

REFERENCES

[1] V. Mor-Avi, L. Sugeng, L. Weinert, P. MacEneaney, E. G. Caiani, R. Koch, I. S. Salgo, R. M. Lang, *Fast measurement of left ventricular mass with real-time three-dimensional echocardiography: comparison with magnetic resonance imaging*, IEEE Transactions on Image Processing, **110**(13) (2004), 1814–1818.

[2] F. Veronesi, C. Corsi, E. G. Caiani, A. Sarti, C. Lamberti, *Tracking of left ventricular long axis from real-time three-dimensional echocardiography using optical flow techniques*, IEEE Trans Inf Technol Biomed, **10**(1) (2006), 174–181.

[3] J. Hansegard, S. Urheim, K. Lunde, S. Malm, S. I. Rabben, *Semi-automated quantification of left ventricular volumes and ejection fraction by real-time three-dimensional echocardiography*, Cardiovasc Ultrasound, **7**(18) (2009), 1–10.

[4] K. Y. E. Leung, J. G. Bosch, *Automated border detection in three-dimensional echocardiography: principles and promises*, Eur J Echocardiogr, **11**(2) (2010), 97–108.

[5] E. D. Angelini, A. F. Laine, S. Takuma, J. W. Holmes, S. Homma, *LV Volume Quantification via Spatiotemporal Analysis of Real-Time 3-D Echocardiography*, IEEE Trans Med Imaging, **20**(6) (2001), 457–469.

[6] M. M. Nillesen, R. G. Lopata, I. H. Gerrits, L. Kapusta, H. J. Huisman, J. M. Thijssen, C. L. de Korte, *Segmentation of the heart muscle in 3-D pediatric echocardiographic images*, Ultrasound Med Biol, **33**(9) (2007), 1453–1462.

[7] O. I. Soliman, B. J. Krenning, M. L. Geleijnse, A. Nemes, J. G. Bosch, R. J. van Geuns, S. W. Kirschbaum, A. M. Anwar, T. W. Galema, W. B. Vletter, F. J. ten Cate, *Quantification of left ventricular volumes and function in patients with cardiomyopathies by real-time three-dimensional echocardiography: a head-to-head comparison between two different semiautomated endocardial border detection algorithms*, J Am Soc Echocardiogr, **20**(9) (2007), 1042–1049.

[8] E. O. Chukwu, E. Barasch, D. G. Mihalatos, A. Katz, J. Lachmann, J. Han, N. Reichek, A. S. Gopal, *Relative importance of errors in left ventricular quantitation by two-dimensional echocardiography: insights from three-dimensional echocardiography and cardiac magnetic resonance imaging*, J Am Soc Echocardiogr, **21**(9), (2008), 990–997.

[9] J. Hansegard, F. Orderud, S. I. Rabben, *Real-time active shape models for segmentation of 3D cardiac ultrasound*, Lect Notes Comput Sci, **4673**, (2007), 157–164.

[10] F. Orderud, S. I. Rabben, *Real-time 3D segmentation of the left ventricle using deformable subdivision surfaces*, Proceedings of Computer Vision and Pattern Recognition, (2008) 1–8.

[11] M. Ma, M. van Stralen, J. H. Reiber, J. G. Bosch, B. P. Lelieveldt, *Model driven quantification of left ventricular function from sparse single-beat 3D echocardiography*, Med Imag Anal, **14**(4) (2010), 582–593.

[12] P. Baraldi, A. Sarti, C. Lamberti, A. Prandini, F. Sgallari, *Evaluation of differential optical flow techniques on synthesized echo images*, IEEE Trans Biomed Eng, **43**(3) (1996), 259–272.

[13] M. Suhling, M. Arigovindan, C. Jansen, P. Hunziker, M. Unser, *Myocardial motion analysis from B-mode echocardiograms*, IEEE Trans Image Process, **14**(4), (2005), 525–536.

[14] M. G. Linguraru, N. V. Vasilyev, G. R. Marx, W. Tworetzky, P. J. Del Nido, R. D. Howe, *Fast block flow tracking of atrial septal defects in 4D echocardiography*, Med Image Anal, **12**(4) (2008), 397–412.

[15] Q. Duan, E. D. Angelini, S. L. Herz, C. M. Ingrassia, K. D. Costa, J. W. Holmes, S. Homma, A. F. Laine, *Region-Based Endocardium Tracking on Real-Time Three-Dimensional Ultrasound*, Ultrasound Med Biol, **35**(2) (2009), 256–265.

[16] K. Y. E. Leung, M. G. Danilouchkine, M. van Stralen, N. de Jong, A. F. van der Steen, J. G. Bosch, *Left ventricular border tracking using cardiac motion models and optical flow*, Ultrasound Med Biol, **37**(4) (2011), 605–616.
[17] J. L. Barron, D. J. Fleet, S. S. Beauchemin, *Performance of optical flow techniques*, Int J Comput Vision, **12**(1) (1994), 43–77.
[18] C. Y. Ahn, *Robust Myocardial Motion Tracking for Echocardiography: Variational Framework Integrating Local-to-Global Deformation*, Computational and Mathematical Methods in Medicine, **2013** (2013), 974027.
[19] A. A. Amini, R. W. Curwen, J. C. Gore, *Snakes and splines for tracking non-rigid heart motion*, Lect Notes Comput Sci, **1065** (1996), 249–261.
[20] M. Li, C. Kambhamettu, M. Stone, *Nonrigid motion recovery for 3D surfaces*, Image Vision Comput, **25**(3) (2007), 250–261.
[21] B. Horn, B. Schunk, *Determining optical flow*, Artif Intell, **17**(2) (1981), 185–203.
[22] B. Lucas, T. Kanade, *An iterative image restoration technique with an application to stereo vision*, in Proc. DARPA IU Workshop, (1981), 121–130.
[23] E. Brusseau, C. L. Korte, F. Mastik, J. Schaar, A. F. Steen, *Fully automatic luminal contour segmentation in intracoronary ultrasound imaging - A statistical approach*, IEEE Trans Med Imaging, **23**(5) (2004), 554–566.
[24] A. Sarti, C. Corsi, E. Mazzini, C. Lamberti, *Maximum likelihood segmentation of ultrasound images with rayleigh distribution*, IEEE Trans Ultrason Ferroelectr Freq Control, **52**(6) (2005), 947–960.
[25] D. Kaplan, Q. Ma, *On the statistical characteristics of log-compressed Rayleigh signals: theoretical formulation and experimental results*, J Acoust Soc Am, **95**(3) (1994), 1396–1400.
[26] G. Slabauh, G. Unal, M. Wels, T. Fang, B. Rao, *Statistical region-based segmentation of ultrasound images*, Ultrasound Med Biol, **35**(5) (2009), 781–795.
[27] D. P. Huttenlocher, G. A. Klanderman, W. J. Rucklidge, *Comparing images using the Hausdorff distance*, IEEE Trans Pattern Anal Machine Intell, **15**(9) (1993), 850–863.
[28] E. Belogay, C. Cabrelli, U. Molter, R. Shonkwiler, *Calculating the Hausdorff distance between curves*, Information Processing Lett, **64** (1997), 17–22.